Initial Reactions in Chemical Vapor Deposition of Ta_2O_5 from $TaCl_5$ and H_2O. An Ab Initio Study

Magdalena Siodmiak,[†] Gernot Frenking,*[,†] and Anatoli Korkin*[,‡]

Fachbereich Chemie, Philipps-Universität Marburg, Hans-Meerwein-Strasse, D-35032 Marburg, Germany, and Computational Technology Lab, Motorola Inc., Mesa, Arizona 85202

Received: July 29, 1999; In Final Form: November 8, 1999

Quantum chemical calculations at the Hartree−Fock, B3LYP, MP2, and CCSD(T) levels of theory were performed in order to study the mechanism of Ta_2O_5 chemical vapor deposition (CVD) from $TaCl_5$ and H_2O. The geometries and vibrational frequencies of reactants, products and transition states of the reactions, which are used for modeling the initial steps of the CVD process were calculated using effective core potentials for Ta and Cl atoms. The reaction between $TaCl_5$ and H_2O proceeds via formation of a strongly bonded six-coordinated tantalum complex (25 kcal/mol at CCSD(T)//B3LYP). The correlated methods show the transition state energy to be close to the energy of the initial reagents. Formation of $TaOCl_3$, in the unimolecular decomposition of $TaCl_4OH$ and $TaCl_3(OH)_2$, has similar barriers of ∼20 kcal/mol. The catalytic effect of an assisting water molecule opens a barrierless channel for $TaOCl_3$ formation in the gas phase.

Introduction

Tantalum pentoxide thin films, a high-quality dielectric material, have been intensively studied for different applications in microelectronic industry, e.g., as capacitors for dynamic random access memories, gate insulator for metal-oxide-semiconductor devices and integrated optical devices[1−8] The high integration of an increasing number of semiconductor devices on chips of decreasing size leads to extremely high requirement of film quality. Among the different growth techniques[9] chemical vapor deposition (CVD)[10] often provides the best quality thin films with very low defect density.[11] The search for optimal precursors and operational conditions in a CVD reactor, e.g., pressure, temperature, carrier gas, flow rate, etc., can be accomplished either experimentally or via computer simulations. Experiments provide the most reliable results, but they are expensive and time and material consuming. Computer simulations are an efficient alternative, if an adequate and reliable model is derived. Gas phase and surface reaction mechanism and kinetics are essential components for the construction of a computer model for CVD reactor simulation. Knowledge of nature, thermochemistry, and kinetics of critical reactions leading to film deposition and to byproduct formation also helps in the search for obtaining high quality thin films with best chemical, electrical, structural, and mechanical properties.

Several precursors such as TaF_5,[12] $TaCl_5$, $Ta[N(CH_3)_2]_5$, $Ta(OCH_3)_5$, and $Ta(OC_2H_5)_5$[13] have been applied in the Ta_2O_5 CVD. Tantalum pentachloride has the advantage of avoiding carbon contamination in growing films.[13] It is also suitable for model experimental and theoretical studies of the CVD mechanism since the number and type of intermediate species and reactions involved are expected to be smaller compared to tantalum compounds with alkylamino and alkoxi ligands. A study of atomic layer deposition (ALD) of Ta_2O_5 from $TaCl_5$ and H_2O revealed important details of the deposition mechanism.[14] Since in ALD the active components are introduced into the reaction zone subsequently, it allows a homogeneous distribution of reactants throughout the surface area. It also separates certain deposition reaction steps, which provides films with high precision thickness control and facilitates the study of the deposition mechanism. According to Aarik and coworkers[14] formation of intermediate volatile $TaOCl_3$ explains etching, which occurs at high $TaCl_5$ doses and increased temperature. The reactivity of $TaCl_5$ toward H_2O-treated tantalum oxide has been shown to be higher than the reactivity of H_2O toward $TaCl_5$-treated oxide surfaces.[14]

There is a growing number of theoretical ab initio studies of molecules (clusters) and their reactions, which provide valuable information about a CVD mechanism of semiconductor and dielectric-type materials for known and potential applications in the microelectronic industry (see, for example, ref 15 and the literature cited therein). Besides fundamental *qualitative* knowledge about the type of reactions which may occur in CVD processes, these studies provide *quantitative* values of thermochemical and kinetics parameters, which can be used in semiempirical modeling of processes in CVD reactors. In this paper we present a quantum chemical study of initial reactions in tantalum pentoxide deposition from the $TaCl_5/H_2O$ system.[16] Although this study concerns only selected reactions of gas-phase molecules, we believe that it helps to understand the molecular mechanism of Ta_2O_5 CVD. We predict that the reaction between $TaCl_5$ and H_2O in the gas phase occurs without a significant barrier. Assuming that fast vibrational energy relaxation occurs on the surface of the growing Ta_2O_5 film, an intermediate complex of hexa-coordinated tantalum can be formed between $TaCl_5$ and hydroxyl groups on the surface. We have used a variety of theoretical methods, i.e., HF, MP2, B3LYP, and CCSD(T) in combination with effective core potentials (ECP) and 6-31G* basis sets. According to the literature data[17] correlated methods in combination with ECP's can provide a reasonable (∼3−5 kcal/mol) accuracy for such reaction energies and barriers. We have also computed heats of formation, structures, and vibrational frequencies of the tantalum

[†] Philipps-Universität Marburg
[‡] Motorola Inc.

10.1021/jp992673d CCC: $19.00
Published on Web 01/25/2000

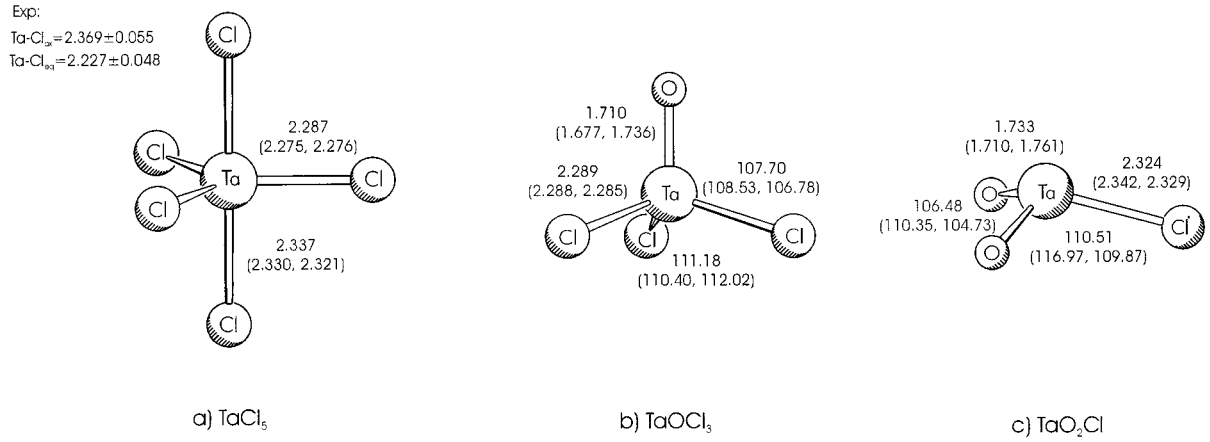

Figure 1. Optimized geometries of (a) $TaCl_5$, (b) $TaOCl_3$, (c) $TaClO_2$ at the B3LYP level. Values at HF followed by MP2 data are given in parentheses. Bond lengths are given in Å, angles in degrees.

TABLE 1: Computed and Experimental Vibrational Frequencies (in cm^{-1}) and IR Intensities (in % to the most active mode) for $TaCl_5$

freq	HF	MP2	B3LYP	exp[a]
$\nu_1(a'_1)$	383 (0)	415 (0)	400 (4)	406
$\nu_2(a'_1)$	294 (0)	330 (0)	319 (0)	324
$\nu_3(a''_2)$	329 (100)	376 (100)	359 (100)	371
$\nu_4(a''_2)$	161 (8)	176 (7)	166 (6)	155
$\nu_5(e')$	371 (55)	413 (50)	399 (54)	402
$\nu_6(e')$	138 (4)	147 (3)	139 (3)	181
$\nu_7(e')$	55 (1)	58 (3)	59 (2)	54
$\nu_8(e'')$	182 (0)	198 (0)	187 (0)	127

[a] Reference 16

containing molecules $TaCl_5$, $TaOCl_3$, TaO_2Cl, $TaCl_4OH$, and $TaCl_3(OH)_2$. In this series of molecules only $TaCl_5$ has been studied experimentally,[18] while theoretical data are available for $TaCl_5$[19] and $TaOCl_3$.[20,21] A comparison of our theoretical results with literature data for these two molecules provides an estimate of the accuracy of ab initio approaches applied in this study, while computational data obtained for unknown tantalum compounds, e.g. TaO_2Cl, $TaCl_4OH$, and $TaCl_3(OH)_2$ should help in their experimental identification and characterization.

Computational Methods

Molecular geometries have been optimized using three different theoretical methods: HF, MP2,[22] and B3LYP[23] as implemented in the *Gaussian 98* program package.[24] Analytical harmonic frequencies have been computed at the B3LYP level of theory for all stationary structures and at the HF and MP2 levels for selected molecules. HF vibrational frequencies are scaled by 0.89.[25] Single point coupled cluster CCSD(T)[26] calculations have been done at the B3LYP optimized geometries. All relative energies presented in the paper include zero-point energy (ZPE) corrections. If not specified otherwise relative energies discussed in the paper are given at the CCSD(T)// B3LYP level and the structural parameters for the B3LYP optimized geometries.

All calculations were performed using a quasi-relativistic effective core potential (ECP) for tantalum with a valence basis set (441/2111/21), which was derived from the [55/5/3] valence basis set of Hay and Wadt.[27] Also, for chlorine, an ECP with a valence basis set (4/5)/[2s3p][28] extended by a d-type polarization function[29] was used. For oxygen and hydrogen atoms we used 6-31G** basis sets.[30] It has been demonstrated for a representative set of transition metal complexes[31] that ECPs generated for ab initio methods can be applied in DFT-based calculations as well. To confirm the accuracy of the ECP in the reaction mechanism study, we performed B3LYP calculations of tantalum oxochloride formation (see below) with a 6-31G* all-electron basis set[30] for the chlorine atom. The difference in the calculated reaction energies using both kinds of basis sets for chlorine atom is only 3 kcal/mol.

Results and Discussion

Considering the mechanism of initial reactions leading to formation of tantalum pentoxide from tantalum pentachloride and water we have computed a series of tantalum-containing molecules: $TaCl_5$, $TaOCl_3$, TaO_2Cl, $TaCl_4OH$, and $TaCl_3(OH)_2$. For $TaCl_4OH$ and $TaCl_3(OH)_2$ several geometric isomers can be visualized based on different possible locations of Cl and OH in a trigonal bipyramide (axial and equatorial) and H-bonding pattern. Since a detailed conformational analysis of tantalum hydroxychlorides is beyond the scope of our paper we have considered only a few geometric isomers and conformations, which apparently have low energies or are located on a minimum energy pathway toward a reaction transition state. Conformational processes in those molecules are accompanied by small energy changes and thus should be very fast.

Structure, Bonding, and Vibrational Frequencies of $TaCl_5$, $TaOCl_3$, and TaO_2Cl. The calculated geometries of $TaCl_5$,

TABLE 2: Computed Harmonic Vibrational Frequencies (in cm^{-1}) and IR Intensities (in % to the most active mode) for $TaOCl_3$ and Experimental Vibrational Frequencies for $VOCl_3$ and $NbOCl_3$

freq	HF	MP2	B3LYP	assignment	$VOCl_3$[a]	$NOCl_3$[b]
$\nu_1(a_1)$	1010 (100)	949 (31)	1017 (100)	TaO bond stretch	1043	997
$\nu_2(a_1)$	372 (9)	405 (13)	398 (10)	TaCl symmetric bond stretch	411	395
$\nu_3(a_1)$	120 (2)	123 (2)	123 (2)	ClTaCl symmetric bending	160	133
$\nu_4(e)$	377 (57)	420 (100)	410 (80)	TaCl asymmetric bond stretch	508	448
$\nu_5(e)$	216 (4)	223 (2)	227 (3)	OTaCl bending	246	225
$\nu_6(e)$	103 (1)	106 (1)	108 (1)	ClTaCl asymmetric bending	124	106

[a] Reference 33. [b] Reference 31, 34.

TABLE 3: Computed Vibrational Frequencies (in cm^{-1}) and Intensities (in % to the most active mode) for TaO_2Cl

freq	HF	MP2	B3LYP	assignment
$\nu_1(a')$	986 (43)	917 (23)	999 (42)	TaO bond symmetric stretch
$\nu_2(a')$	367 (25)	390 (61)	392 (34)	TaCl stretch
$\nu_3(a')$	293 (3)	316 (5)	329 (4)	OTaO bending
$\nu_4(a')$	102 (28)	155 (28)	156 (20)	$ClTa(O_2)$ symmetric bending
$\nu_5(a'')$	925 (100)	904 (100)	946 (100)	TaO bond asymmetric stretch
$\nu_6(a'')$	153 (2)	176 (<1)	180 (<1)	$ClTa(O_2)$ asymmetric bending

TABLE 4: Results of the NBO Analysis at B3LYP: Bond Polarity (%Ta), Relative Contribution of s, p, and d Orbitals of Tantalum, and Atomic Charges (q)

bond	%Ta	%s (Ta)	%p (Ta)	%d (Ta)	q(Ta)	q(O)	q(Cl)
			$TaOCl_3$ C_{3v}				
TaCl	18	27	1	72	1.66	−0.71	−0.32
TaO σ	21	18	1	81			
TaO π^a	23	0	1	99			
			TaO_2Cl C_{2v} (planar)				
TaCl	8	68	10	23	2.23	−0.83	−0.56
TaO σ	15	4	12	84			
TaO $\pi_\perp$	26	0	3	97			
TaO $\pi_{\|\|}$	11	5	26	69			
			TaO_2Cl C_s (nonplanar)				
TaCl	14	50	2	48	2.06	−0.79	−0.47
TaO σ	18	19	8	74			
TaO π_1	24	3	3	95			
TaO π_2	13	1	29	70			

[a] There are two degenerated π orbitals in the C_{3v} symmetric $TaOCl_3$.

TABLE 5: Relative Energies of $TaCl_4OH$ and $TaCl_3(OH)_2$ Conformers (in kcal/mol)

	HF	MP2	B3LYP	CCSD(T)
$TaCl_4OH$				
OH-eq	0.0	0.0	0.0	0.0
TS	1.9	1.9	2.0	1.9
OH-ax	1.2	0.9	1.1	0.9
$TaCl_3(OH)_2$				
OH, OH-eq	0.0	0.0	0.0	0.0
TS	2.8	2.9	2.8	3.1
OH-eq, OH-ax	1.3	0.4	0.8	0.9

$TaOCl_3$, and TaO_2Cl at B3LYP, HF, and MP2 are shown at Figure 1. The corresponding vibrational frequencies are presented in Tables 1−3. Experimental data are available only for $TaCl_5$.[18] The experimental value for the equatorial TaCl bond length (2.227 Å) is shorter and for the axial bond it is longer (2.369 Å) than the corresponding calculated values. However, the computational values are within standard deviations estimated for the experimental values (see Figure 1a). The B3LYP method provides longer axial and equatorial bonds compared to the other two computational approaches, HF and MP2. In an earlier ab initio HF pseudopotential study of $TaCl_5$, values of 2.369 Å and 2.326 Å were reported for the axial and equatorial TaCl bonds, respectively.[19] The B3LYP calculation of $TaCl_5$ with a 6-31G* basis set for chlorine atom gives a bond length of 2.346 Å for the axial Ta−Cl bond, which is close to the experimental value. The calculated equatorial Ta−Cl bond length (2.290 Å) has a larger deviation from experiment.

The computed and experimentally assigned[18] vibrational frequencies of $TaCl_5$ are in good agreement except for ν_6 and ν_8, where theory and experiment show opposite values. Similar disagreement between theory and experiment in the symmetry assignment of these two modes has been pointed by Albright et al.[19] The e″ mode is formally symmetry forbidden, but coupling of vibrational modes may let the ν_8 mode mix with other vibrations. This may lead to an erroneous symmetry assigment based on experimental IR and Raman intensities. Our calculated value of 1.7 kcal/mol for the energy of pseudorotation barrier in $TaCl_5$ computed at B3LYP coincides with an earlier estimate at QCISD(T).[19] It is also in good agreement with an experimental value of 1.2 kcal/mol[18] estimated using electron diffraction data obtained at 100 °C.

SCHEME 1

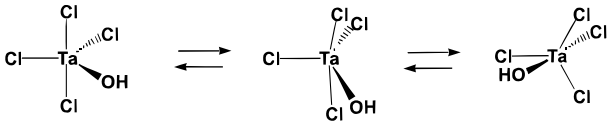

SCHEME 2

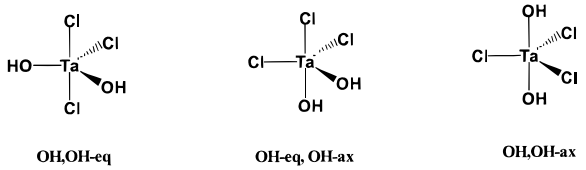

SCHEME 3

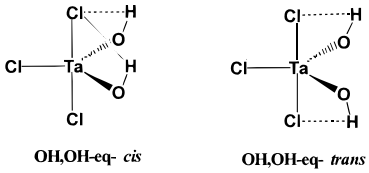

There are no experimenatal data available for the geometries and vibrational frequencies of $TaOCl_3$. Our calculated molecular geometries (Figure 1b) can be compared only with the data obtained from earlier theoretical studies at Hartree−Fock and MP2[20] and at the DFT (local density approximation (LDA))[21] levels of theory. In our and other calculations the ∠OTaCl angle is smaller than ∠ClTaCl in $TaOCl_3$. Similar results were obtained for the other group 5 oxychlorides, $VOCl_3$21[32] (∠OVCl = 107.6°, ∠ClVCl = 111.3°) and $NbOCl_3$21,[33] (∠ONbCl = 106.0°, ∠ClNbCl = 112.7°). This is in contrast to main-group 15 oxochlorides, e.g., $POCl_3$ (∠OPCl = 114.8°, ∠ClPCl = 103.7°).[34] The calculated harmonic frequencies for $TaOCl_3$ are given in Table 2 along with experimental frequencies for $VOCl_3$[35] and $NbOCl_3$.[33,36] The frequency pattern is very similar for all three molecules. Vibrational frequencies diminish with increasing atomic mass ($\omega \sim M^{-1/2}$) and the reduced masses of vibrations approach the masses of light ligand atoms, O or Cl, if the mass of the central heavy atom grows. According to this we may simply extrapolate the $TaOCl_3$ vibrational frequencies to be 10−20 cm^{-1} smaller than the corresponding values for $NbOCl_3$.

An NBO analysis for $TaOCl_3$ at B3LYP is presented in Table 4. The Ta−Cl and Ta−O bonds are very polar. The σ and π bonds have a maximum localization of only 26% at the tantalum end. Thus, Ta always carries a large positive charge. The metal s orbital contributes more to the Ta−Cl bonds than to the Ta−O σ bonds.

There are neither theoretical nor experimental data available for TaO_2Cl. According to our computations the molecule is nonplanar with Ta−Cl and Ta−O bond lengths being larger than in $TaOCl_3$. The nonplanar structure is a result of a compromise between ligand−ligand repulsion, which would lead to a planar structure, and the overlap between metal and ligand orbitals, which according to Landis[37] favors angles smaller than 120° for any sd^n hybridization. If the planar structure is imposed in the geometry optimization, all bonds become longer (TaO = 1.737 Å, TaCl = 2.361 Å) and the energy raises by 5.7 kcal/mol at B3LYP.

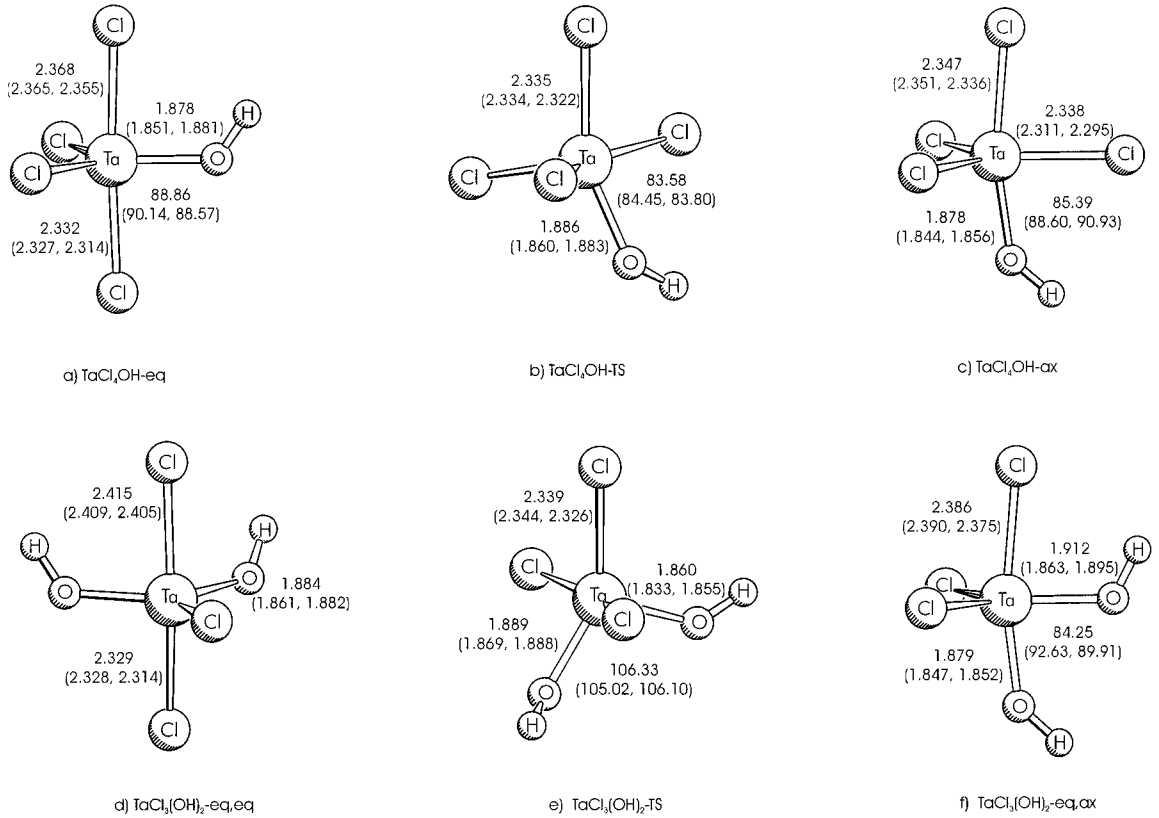

Figure 2. Optimized geometries of $TaCl_4OH$ and $TaCl_3(OH)_2$ conformers at the B3LYP level. Values at HF followed by MP2 data are given in parentheses. Bond lengths are given in Å, angles in degrees.

TABLE 6: Zero Kelvin Heats of Initial Reactions of $TaCl_5$ Hydrolysis and Ta_2O_5 Deposition (in kcal mol)[a]

reaction	HF	MP2	B3LYP	CCSD(T)
(1) $TaCl_5 + H_2O \rightarrow TaCl_4OH + HCl$	−8.0	−7.6	−8.6	−7.3
(2) $TaCl_4OH + H_2O \rightarrow TaCl_3(OH)_2 + HCl$	−8.0	−6.8	−7.4	−6.8
(3) $TaCl_4OH \rightarrow TaOCl_3 + HCl$	11.7	0.1	9.2	8.0
(4) $TaCl_3(OH)_2 \rightarrow TaOCl_3 + H_2O$	19.7	6.9	16.6	14.9
(5) $TaOCl_3 + H_2O \rightarrow TaO_2Cl + 2HCl$	90.0	76.6	78.7	82.0

[a] Lower energy conformers of $TaCl_4OH$ and $TaCl_3(OH)_2$ have been used used in computation of heats of reactions 1−4.

TABLE 7: Estimated Heats of Formation and Ta−O Bond Dissociation Energies in Tantalum-Containing Molecules

	$TaCl_4OH$	$TaCl_3(OH)_2$	$TaOCl_3$	TaO_2Cl
$\Delta H°_f$ [kcal/mol]	−225.8	−268.3	−195.7	−127.3
E_{TaO} [kcal/mol]	126.4	126.1	220.5	179.8

In accord with the bond elongation in TaO_2Cl, the corresponding Ta−O and Ta−Cl bond stretch vibrations have lower frequencies compared to $TaOCl_3$ (see Table 3). The predicted IR spectrum of TaO_2Cl has four intense bands: two modes around 1000 cm^{-1}, which correspond to symmetric and asymmetric Ta−O bond stretching, one mode with a frequency 370 cm^{-1} corresponding to Ta−Cl bond stretching mixed with ∠OTaO bond angle bending. Finally, the vibration at about 100 cm^{-1} corresponds to the ∠TaOCl bond angle bending.

The NBO analysis (see Table 4) shows a similar Ta hybridization character in the σ(Ta−O) and Ta−Cl bonds of $TaOCl_3$, while in TaO_2Cl the Ta d-orbitals dominate in the σ-(Ta−O) bonds and the s-orbital mainly contributes to the Ta−Cl bond. In the nonplanar TaO_2Cl molecule the Ta AO has almost exact sd hybridization in the TaCl bond. There is a significant difference between the charge distribution in the planar and nonplanar form of TaO_2Cl. In the nonplanar form the Ta atom is less positive (+2.06) than in the planar form (+2.23). Thus, bending of the molecule increases the covalent contribution to the chemical bonding in TaO_2Cl.

Energies and Structures of $TaCl_4OH$ and $TaCl_3(OH)_2$. Tantalum hydroxytetrachloride [$TaCl_4OH$] and tantalum dihydroxytrichloride [$TaCl_3(OH)_2$] are intermediate species in the hydrolysis of tantalum pentachloride yielding tantalum pentoxide. Two geometric isomers can be visualized for $TaCl_4OH$, with equatorial and axial positions of the hydroxyl group, respectively. The two isomers apparently can be converted into each other via a square pyramidal transition state (Berry pseudorotation), Scheme 1.

We located both geometric isomers and the energetically low lying transition state shown in Scheme 1 (see Figure 2 a−c and Table 5). The isomer with an equatorial position of the OH group (Figure 2a) is more stable. All methods predict that the OH-ax isomer (see Figure 2c) is ca. 1 kcal/mol higher in energy. The barrier for interconversion of OH-eq into OH-ax is ∼2 kcal/mol. In all three structures the OH group forms an H-bond with the nearest chlorine atom. The average OH···Cl *intramolecular* H-bond distance is 2.932 Å at B3LYP, which can be compared with 2.56 (2.57) Å *intermolecular* H-bond in $(HCl)_2$ dimer computed at the B3LYP (MP2) level with the 6-31+G** basis set.[38] According to Del Bene et al.[38] the B3LYP method somewhat overestimates binding energies of H-bonds and gives shorter than experimental bond distances, particularly for small basis sets.

For $TaCl_3(OH)_2$, the product of the second step of $TaCl_5$ hydrolysis, we can visualize three isomers with respect to the position of OH and Cl in the trigonal bipyramide (Scheme 2).

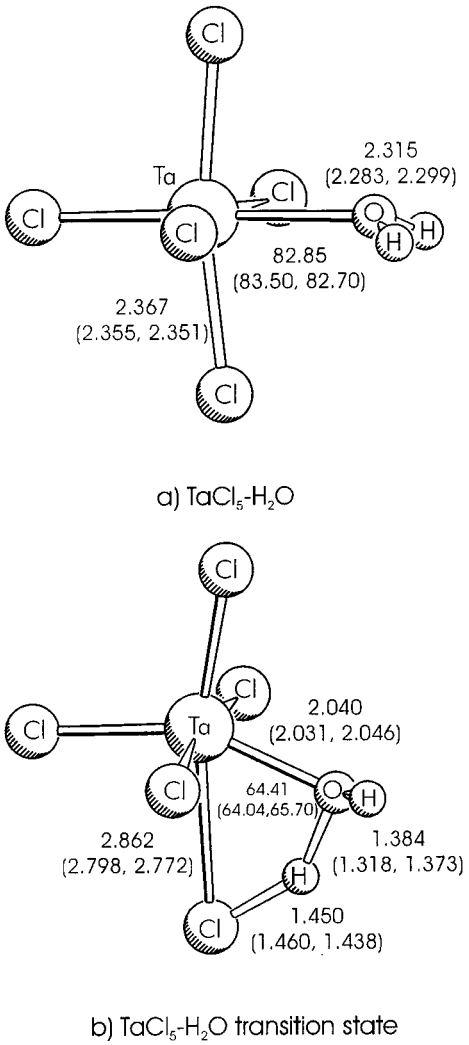

Figure 3. Geometries of $TaCl_5-H_2O$ complex and $TaCl_5-H_2O$ transition state optimized at the B3LYP level. Values at HF followed by MP2 data are given in parentheses. Bond lengths are in Å, angles are given in degrees.

We have computed all three isomers at the B3LYP level. As expected from the results of the $TaCl_4OH$ computations, stability of isomers with axial OH groups is lower. Thus the relative energy of the least stable isomer with two axial OH groups (**OH,OH-ax**) is 1.8 kcal/mol above the energy of the most stable isomer with two equatorial OH groups (**OH,OH-eq**). We have computed only the first two geometric isomers in Scheme 2 and the transition state between them at all four levels of theory (see Figure 2d−f and Table 5). The barrier for pseudorotation is ∼3 kcal/mol for $TaCl_3(OH)_2$, which is 1 kcal/mol higher than the barrier in $TaCl_4(OH)$. According to the results derived for $TaCl_4OH$, two patterns in the H-bond should be favorable (Scheme 3).

We have found at B3LYP that the trans H-bond conformation is less favorable than the cis conformation by 0.7 kcal/mol. Since an extensive conformational analysis is beyond of the scope of our paper we have not considered the trans H-bond conformation.

Thermochemistry of Gas-Phase Reactions in the System $TaCl_5/H_2O$. Hydrolysis of $TaCl_5$ and deposition of Ta_2O_5 include a series of elementary reactions of substitution of chlorine by oxygen in the coordination sphere of tantalum. We have computed some initial reactions between $TaCl_5$ and H_2O, which may occur in the tantalum pentoxide CVD process in the gas phase or on the growing Ta_2O_5 surface terminated by Cl and OH groups. Zero Kelvin heats of reactions are presented in Table 6. The first and second steps of $TaCl_5$ hydrolysis have similar reaction energies at all levels of theory. Since the coordination of tantalum remains the same on the left and right sides in eqs 1 and 2, correlation effects probably compensate in the reaction energies of the two reactions. Such a compensation effect is not observed in the last three reactions, where the coordination number of Ta becomes lower in the reaction course and strong correlation effects may be expected. Note that even in the nonisodesmic eqs 3−5 in Table 6 the B3LYP reaction energies are close to CCSD(T) values within a 3 kcal/mol range, while MP2 values differ by about 8 kcal/mol from CCSD(T).

While the substitution of Ta−Cl bonds by Ta−OH in reactions 1 and 2 is *exothermic*, the formation of a Ta═O double bond is *moderately endothermic* in reactions 3 and 4 and

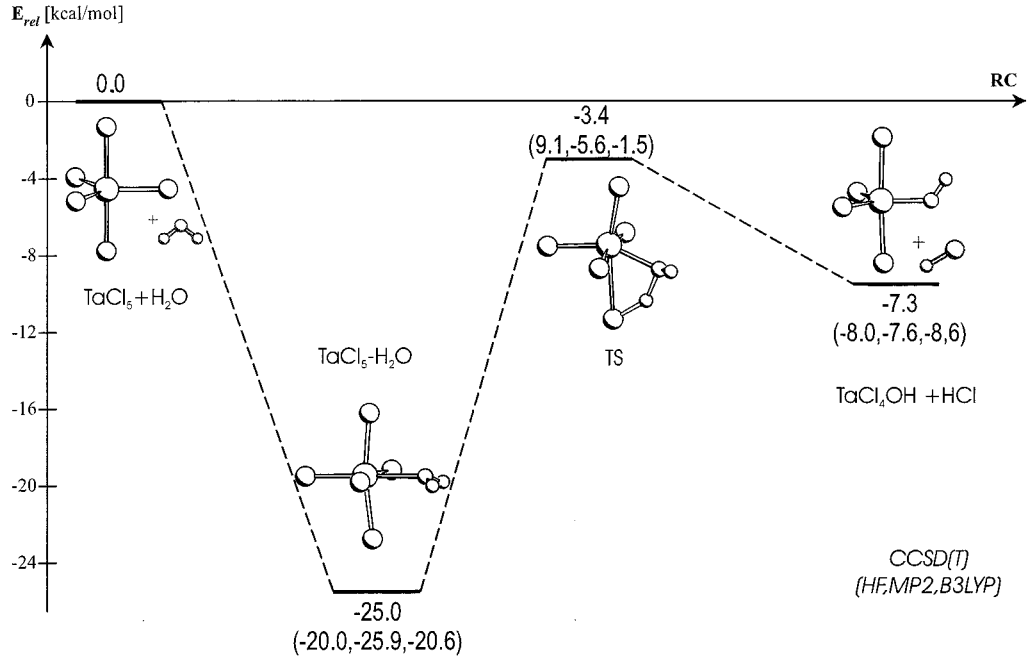

Figure 4. Calculated reaction path for the hydrolysis of $TaCl_5$ at CCSD(T). Relative energies at HF, MP2, and B3LYP are given in parentheses.

strongly endothermic in reaction 5, which certainly makes tantalum oxychlorides, particularly TaO_2Cl, difficult for experimental observation. The B3LYP calculation of the energy of the reaction $TaCl_5 + H_2O \rightarrow TaCl_3O + 2HCl$ (sum of the energies of reactions 1 and 3 in Table 6) using a 6-31G* basis set for chlorine gives 3.6 kcal/mol which is in reasonable agreement with 0.6 kcal/mol obtained in the calculations using an ECP for Cl.

The calculated reaction energies presented in Table 6 allow to estimate heats of formation of all tantalum-containing molecules in Table 6, based on $\Delta H°_f$ values available for $TaCl_5$ (−182.8 kcal/mol), H_2O (−57.8 kcal/mol), and HCl (−22.1 kcal/mol)[39] (see Table 7). For the estimation of the heats of formation we used the most reliable CCSD(T) values for the reaction energies. Using these data and known heats of formation[39] for gaseous Ta (186.9 kcal/mol), Cl (29.0 kcal/mol), O (59.6 kcal/mol), and OH (9.3 kcal/mol) we can also estimate the Ta−O bond dissociation energies using a simple additivity approach and the assumption that the Ta−Cl bonds have the same (average) energy of 102.9 kcal/mol in all tantalum-containing molecules, which can be estimated from the heat of atomization of $TaCl_5$ (Table 7). It is seen that the Ta−O single bond energies are similar in $TaCl_4OH$ and in $TaCl_3(OH)_2$, which can be (tentatively) used for validating an additivity approach in calculating bond energies in other $TaCl_x(OH)_{5-x}$ molecules. Note that the Ta═O double bond in $TaOCl_3$ has a higher bond energy than in TaO_2Cl, indicating a partial triple bond character in C_{3v} symmetric oxotrichloride. The computed TaO bond energies can also be compared with Ta−C (67 kcal/mol), Ta═C (126 kcal/mol), and Ta−I (62.9 kcal/mol) avarage bond energies.[40] Probably the ionic character makes the TaO bond much stronger than the less polar (more covalent) TaC and TaI bonds. This is particularly displayed in the Ta−O *single* bond, which is predicted to have similar bond energy as the Ta═C double bond.

Assuming that the further hydrolysis steps have similar (∼ −7 kcal/mol) reaction energies as for reactions 1 and 2 in Table 6, we may use the difference in the estimated heats of formation for $TaCl_4OH$ and $TaCl_3(OH)_2$ as an increment to calculate $\Delta H°_f$ for completely hydrolyzed $Ta(OH)_5$. This gives a value of $\Delta H°_f = -395.8$ kcal/mol, which can be used further to estimate the heat of reaction for conversion of hypothetical gaseous $Ta(OH)_5$ into solid Ta_2O_5:

$$2Ta(OH)_5 \rightarrow Ta_2O_5 + 5H_2O \quad \Delta H°_r = 13.6 \text{ kcal/mol}$$

A calculation based on tabulated heats of formation of gaseous $TaCl_5$ and H_2O and solid Ta_2O_5 (−489.0 kcal/mol)[39] gives a negative (exothermic) value of the reaction heat for the formation of Ta_2O_5:

$$2TaCl_5 + 5H_2O \rightarrow Ta_2O_5 + 10HCl \qquad \Delta H°_r = -55.4 \text{ kcal/mol}$$

Entropy effects favor formation of tantalum pentoxide for both reactions, particularly at higher temperatures applied in CVD.

Although thermodynamic calculations are important in estimating the "chemical driving force", energy balance and relative stability of the intermediates, and products of deposition, in most cases CVD processes occur at conditions which are far from thermodynamic equilibrium. The film structure and composition are governed by other factors: chemical kinetics, surface and gas diffusion, and mass transfer. To reveal important details of potential energy surfaces for the types of reactions which may occur in tantalum pentachloride CVD, we have computed transition states and intermediate complexes for the first step

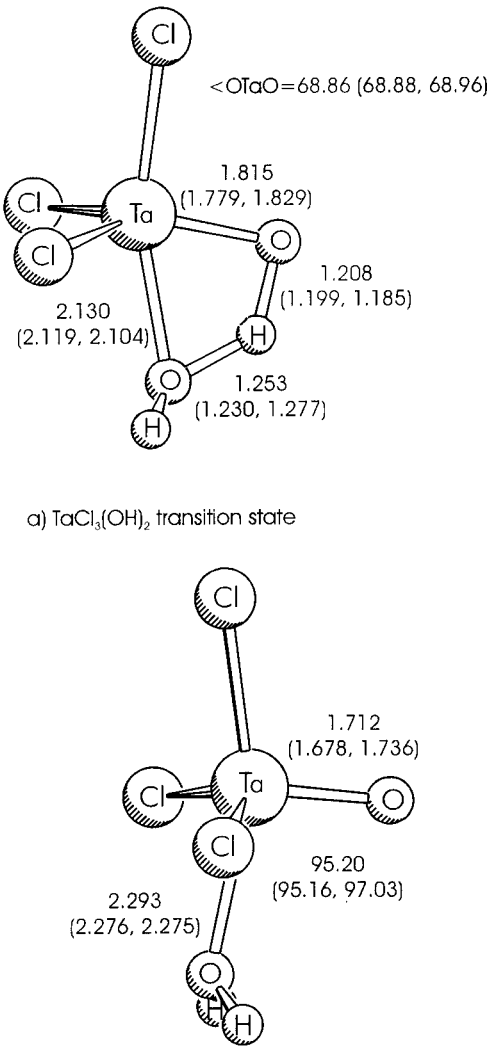

Figure 5. Geometries of the $TaOCl_3-H_2O$ transition state and the $TaOCl_3-H_2O$ complex optimized at B3LYP. Values at HF followed by MP2 data are given in parentheses. Bond lengths are in Å, angles are given in degrees.

of $TaCl_5$ hydrolysis (eq 1 in Table 6) and for $TaCl_3(OH)_2$ dehydration and for $TaCl_4OH$ dehydrochlorination (eqs 1, 4, and 3, respectively, in Table 6).

Mechanism of Hydrolysis of $TaCl_5$. High valent transition metal compounds easily form complexes with electron donors increasing the coordination number of the central atom. According to our calculated results $TaCl_5$ forms a strong donor−acceptor complex with H_2O (see Figure 3a and Figure 4). The stabilization energy of the complex varies within a 6 kcal/mol range between 20 kcal/mol value at HF and 26 kcal/mol at MP2, with the B3LYP value being close to the HF value and MP2 matching CCSD(T). The Ta−O distance in the $TaCl_5-H_2O$ complex is about 0.5 Å longer than in tantalum hydroxychlorides: $TaCl_4OH$ and $TaCl_3(OH)_2$ (Figure 2). The calculated 2.315 Å at B3LYP can be compared with the experimental Ta−OH_2 distance in Cp*Ta(OH2)(p-*tert*-butylcalix[4]arene), which is equal to 2.188 Å.[41]

The transition state energy in the reaction of $TaCl_5$ hydrolysis is lower than the energy of the separated $TaCl_5$ and H_2O molecules at all but the HF level. Overestimation of the reaction barrier is typical for the Hartree−Fock method, while B3LYP and CCSD(T) give similar barriers within a reasonable 3 kcal/

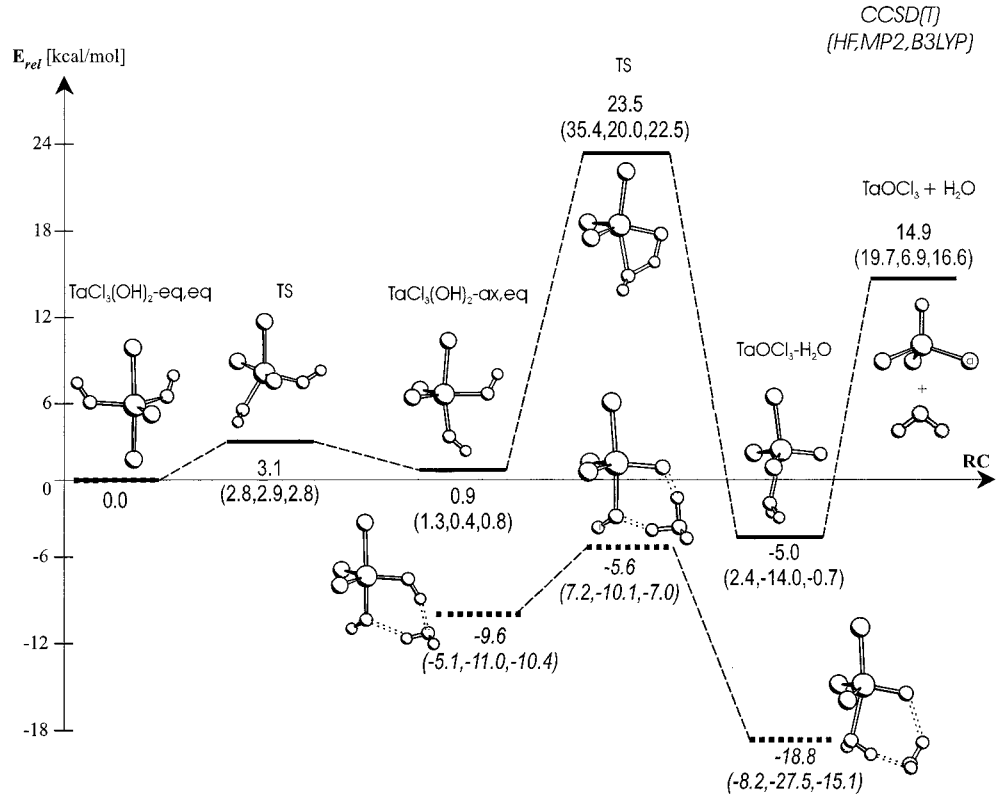

Figure 6. Calculated reaction path for the dehydration of $TaCl_3(OH)_2$ at CCSD(T) without (top) and with (bottom) water assistance. Relative energies at HF, MP2, and B3LYP are given in parentheses. Relative energies for the water-assisted reaction are calculated with respect to separated $TaCl_3(OH)_2$ and H_2O molecules.

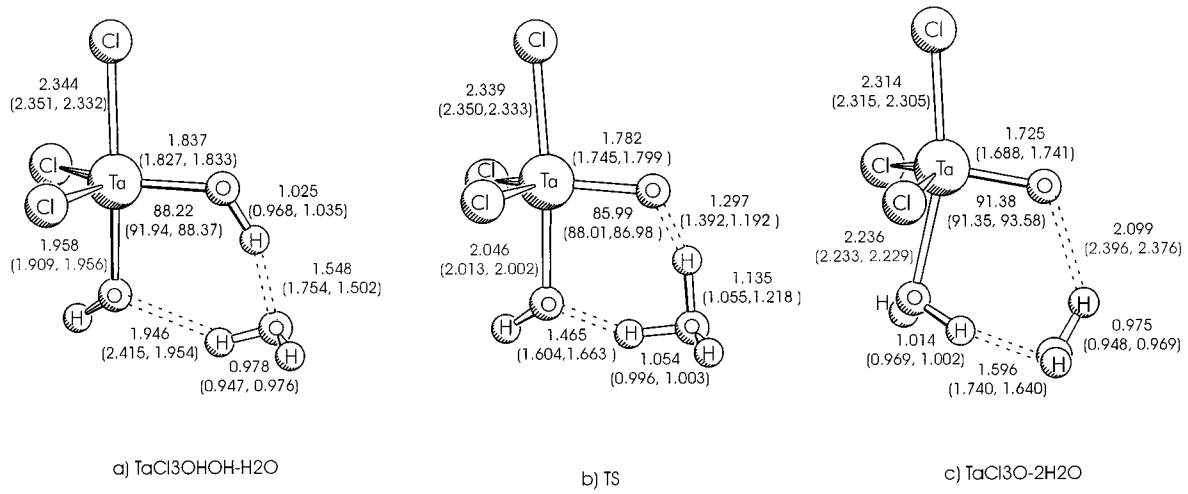

Figure 7. B3LYP optimized geometries of $TaCl_3(OH)_2$, transition state and $TaCl_2O-H_2O$ complexes with assisting water molecule. Values at HF followed by MP2 data are given in parentheses. Bond lengths are in Å, angles are given in degrees.

mol range. Thus our calculations predict that in the gas phase $TaCl_5$ hydrolysis should occur without a barrier. However, considering the same reaction of $TaCl_5$ adsorbed on the surface (or similar reaction for a $TaCl_x$ surface fragment), we must take into account the surface as a part of the reacting system. The energy released in formation of $TaCl_5-H_2O$ complex (~26 kcal/mol) dissipates in surface and bulk film vibrational modes. Thus the barrier for the reaction on the surface is not equal to the energy difference between separated $TaCl_5/H_2O$ and the transition state but the one between $TaCl_5-H_2O$ complex and TS (~20 kcal/mol).

The Ta−Cl distance in the transition state (see Figure 3b), which corresponds to a leaving Cl atom, is about 0.5 Å longer than in the $TaCl_5-H_2O$ complex, while the Ta−O distance is intermediate between the values in the complex and in $TaCl_4$-OH.

We have not been able to locate a $TaCl_4OH-HCl$ complex with six-coordinated tantalum on a "product site" similar to the $TaCl_5-H_2O$ complex on the "reactant site". At each level the optimization did collapse to a hydrogen bonded form of $TaCl_4$-OH···ClH without formation of a donor−acceptor bond between Ta and Cl.

We calculated next the structures and energies along the path of hydrolysis of tantalum hydroxytetrachloride. $TaCl_4OH$ forms a strong complex with water (−21.6 kcal/mol at B3LYP), in which H_2O is positioned at the backside of the OH group. The

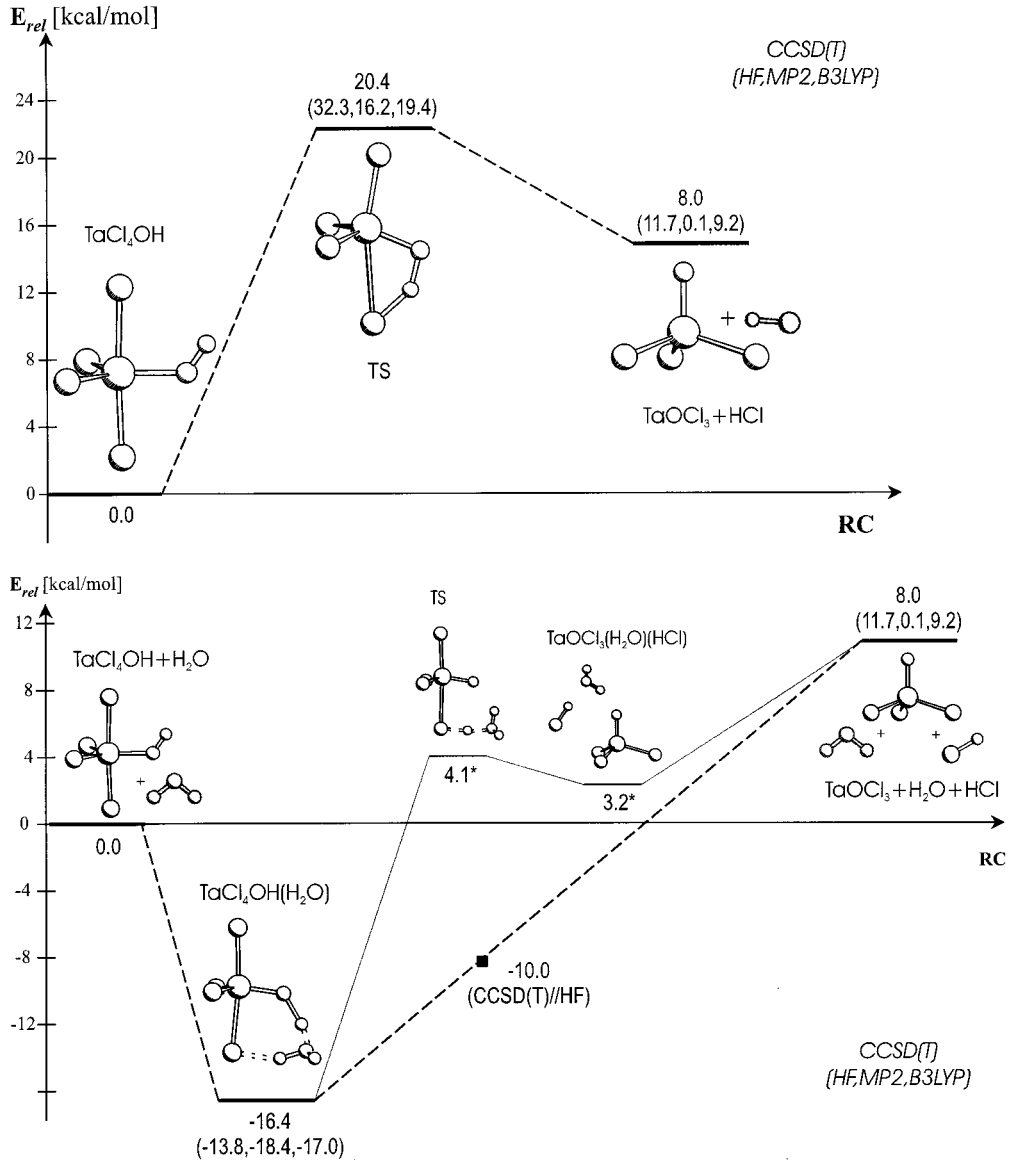

Figure 8. Calculated reaction path for the dehydrochlorination of $TaCl_4OH$ at CCSD(T): (a) direct decomposition (b) water assisted reaction. Relative energies at HF, MP2, and B3LYP are given in parentheses.

Ta−O bond length in $TaCl_4OH-H_2O$ is 2.289 Å at B3LYP, which is 0.026 Å shorter than in $TaCl_5-H_2O$. The hydrolysis of $TaCl_4OH$ proceeds similar to the hydrolysis of $TaCl_5$ with transition state energy close to the energies of separated $TaCl_4$-OH and H_2O molecules: −2.4 kcal/mol at B3LYP.

Mechanism of Dehydration of Tantalum $TaCl_3(OH)_2$. The termination of tantalum pentoxide film surface by the OH group is most plausible under atmospheric condition or exposure to water under deposition condition, which include H_2O as a precursor (oxygen source). According to Aarik and co-workers[14] the film etching, which occurs at higher $TaCl_5$ concentrations and elevated temperature, can be explained by the formation of intermediate volatile tantalum oxychlorides, e.g., $TaOCl_3$. Formation of TaO_2Cl is unfavorable because of a very high endothermicity for its formation (see Table 6).

We optimized the stationary structures, minima, and transition states, for $TaOCl_3$ formation from $TaCl_3(OH)_2$ (Figure 2d−f and Figure 5). The most stable isomer of $TaCl_3(OH)_2$ (both OH− groups in equatorial positions, Figure 2d) was used as the starting point of the study of dehydration of tantalum dihydroxytrichloride. However, the direct minimum energy path from the transition state (see Figure 6) to the reactant shows that another isomer with one axial and one equatorial OH group (Figure 2f) is the direct product of the reverse reaction. We have found computationally a transition state between two $TaCl_3(OH)_2$ isomers (Figure 2e), which is discussed above. Since the transition state between the $TaCl_3(OH)_2$ isomers has a much lower energy than the transition state for H_2O elimination, Berry pseudorotation does not play a significant role in the reaction of $TaCl_3(OH)_2$ dehydration and can be ignored in most of the kinetics modeling studies.

Also $TaOCl_3$ forms a strong complex with water with a stabilization energy at ∼20 kcal/mol. The water molecule is positioned trans to the Ta−Cl bond. The relative energy of $TaOCl_3-H_2O$ with respect to $TaCl_3(OH)_2$ depends substantially on the computational method. MP2 shows the largest deviation from CCSD(T).

Since in a $TaCl_5/H_2O \rightarrow Ta_2O_5$ CVD process water vapor is used as a precursor, we have also considered the dehydration of $TaCl_3(OH)_2$ assisted by one water molecule. The catalytic effect of external H_2O is provided by increasing polarity (microsolvation) and decreasing the strain in the transition state for dehydration. The energy of two H-bonds in the intermediate $TaCl_3(OH)_2-H_2O$ complex (see Figures 6 and 7a) is 9.6 kcal/

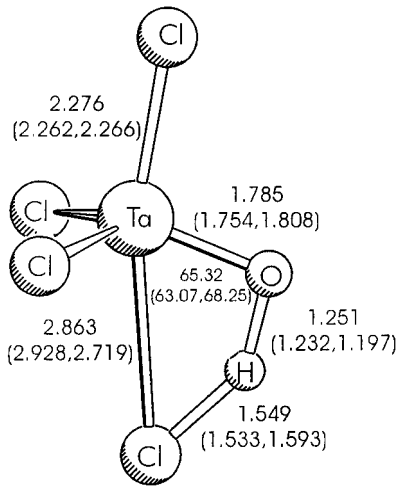

a) $TaCl_3O$-HCl transition state

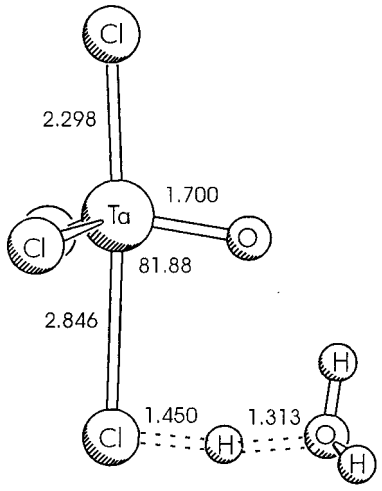

b) $TaCl_3O$-HCl transition state with assisting water*

Figure 9. B3LYP optimized geometries of the transition states for elimination of HCl from $TaCl_4OH$ in (a) direct decomposition (b) water assisted reaction. Values at HF followed by MP2 data are given in parentheses; *values only at the HF level. Bond lengths are in Å, angles are given in degrees.

mol at CCSD(T). The transition state in the H_2O assisted dehydration of $TaCl_3(OH)_2$ (Figure 7b) qualitatively corresponds to the complex of negatively charged $TaCl_3(OH)O^-$ with H_3O^+ cation. The actual NBO charge transfer between these two fragments is 0.69 electrons in NBO analysis. The barrier for the water-assisted hydrogen transfer to $TaCl_3O-H_2O$ complex is now reduced from 22.6 kcal/mol to 4 kcal/mol at CCSD(T). Such phenomenon of microsolvation in the gas phase has already been reported.[42]

Mechanism of HCl Loss of $TaCl_4OH$. Another reaction which may lead to the formation of $TaOCl_3$ is dehydrochlorination of $TaCl_4OH$ (reaction 3 in Table 6). This reaction presents a simplified model of HCl chemical desorption from the Ta_2O_5 surface. We have studied a unimolecular (direct) and bimolecular (water assisted) decomposition of $TaCl_4OH$ into $TaOCl_3$ and H_2O. The energy diagrams for both reactions are shown on Figure 8. The barriers for a unimolecular decomposition of $TaCl_4OH$ with HCl elimination (20.4 kcal/mol) and $TaCl_3(OH)_2$ with H_2O elimination (23.5 kcal/mol) are similar. In the transition state for the HCl elimination (see Figure 9a) the TaCl bond is elongated by ~0.5 Å. Compared to the equilibrium positions in HCl (1.295 Å) and in $TaCl_4OH$ (0.968 Å) the corresponding ClH and OH bond lengths are elongated by 0.354 and 0.283 Å, respectively.

Water assistance significantly reduces the reaction barrier for HCl elimination from $TaCl_4OH$. However, in contrast to the $TaCl_3(OH)_2/H_2O$ system, where the transition state structure resembles the complex of $TaCl_3(OH)O^-$ with H_3O^+ (Figure 7b), the TS for water assisted HCl elimination is product-like (see Figure 9b) and closely corresponds to the H-bonded complex of $TaCl_3O$, H_2O, and HCl. We have only located the TS for H_2O assisted HCl elimination at the HF level. The dominating component in the imaginary frequency vector corresponds to the proton transfer between H_2O and HCl, while the corresponding vector in the TS for water assisted H_2O elimination from $TaCl_3(OH)_2$ shows synchronous motion of two protons.

Neither transition state nor the subsequent H-bonded complex of $TaCl_3O/H_2O/HCl$ has been located at the correlated levels, B3LYP and MP2 (Figure 8b). We believe that the water assisted decomposition of $TaCl_4OH$ occurs without a barrier, when correlation energy is included. This is also (indirectly) confirmed by a very low single point CCSD(T) energy (−10 kcal/mol) computed at the HF optimized structure of the TS (see Figure 9b).

Summary and Conclusion

The results of our theoretical investigation can be summarized as follows:

1. The calculated geometries and vibrational frequencies of the high-valent tantalum compounds which are predicted at the HF, MP2, and B3LYP levels of theory are in good agreement with experimental results of known species. The reaction energies and complex formation energies which are obtained at the CCSD(T) and B3LYP levels do not exhibit large deviations from each other, while the MP2 energies appear to be less reliable.

2. The experimentally yet unknown compounds $TaOCl_3$ and TaO_2Cl have been characterized theoretically. The formation of TaO_2Cl from $TaCl_5$ and $TaOCl_3$ is a thermodynamically disfavored process.

3. The calculations predict that $TaCl_5$ hydrolysis in the gas phase should take place with a small or no barrier at all. The first step of the reaction is the formation of strongly bonded water complex, which eliminates HCl with a substantial barrier with respect to the complex.

4. Water loss from $TaCl_3(OH)_2$ and HCl loss from $TaCl_4OH$ have been studied as model reactions for etching of Ta_2O_5 films at high $TaCl_5$ concentrations at elevated temperatures. Both reactions have large barriers for the unimolecular pathway. The activation barrier becomes much lower through the catalytic assistance of a water molecule, which opens a barriereless reaction channel for reactions in the gas phase. $TaOCl_3$ forms a strong water complex like $TaCl_5$ does with a similar complex formation energy. The role of the assisting water molecule in the etching process is emphasized.

Acknowledgment. This work was supported by the Deutsche Forschungsgemeinschaft (Graduiertenkolleg Metallorganische Chemie). We acknowledge excellent service and generous allotment of computer time of the Computational Technology Lab at Semiconductor Products Sector, Motorola, HRZ Marburg and HHLRZ Darmstadt.

References and Notes

(1) Yun, J. H.; Rhee, S. W. *Thin Solid Films* **1997**, *292*, 324.

(2) McKinley, K. A.; Sandler, N. P. *Thin Solid Films* **1996**, *290*−*291*, 440.
(3) Rausch, N.; Burte, N. P. *Microelectron. J.* **1993**, 421.
(4) Treichel, H.; Mitwalsky, A.; Sandler, N. P.; Tribula, D.; Kern, W.; Lane, A. P. *Adv. Mater. Opt. Electron.* **1992**, *1*, 299.
(5) Tanimoto, S.; Matsui, M.; Aoyagi, M.; Kamisako, K.; Kuroiwa, K.; Tarui, Y. *Jpn. J. Appl. Phys.* **1991**, *30*, L330.
(6) Zaima, S.; Furuta, T.; Yasuda, Y.; Lida, M. *J. Electrochem. Soc.* **1990**, *137*, 1297.
(7) Nishioka, Y.; Shinriki, H.; Mukai, K. *J. Electrochem. Soc.* **1987**, *134*, 410.
(8) Ingrey, S. J.; Westwood, Y. C.; Cheng, Y. C.; Wei, J. *Appl. Opt.* **1975**, *14*, 2194.
(9) (a) Wold, A.; Bellavance, D. In *Preparative methods in solid-state chemistry*; Hagenmuller, P., Ed.; Academic Press: New York, 1972. (b) Müller-Buschbaum, Hk. *Angew. Chem., Int. Ed. Engl.* **1981**, *20*, 22.
(10) Schäfer, H. *Chemical transport reactions*; Academic Press: New York, 1964.
(11) Suntola, T. In *Handbook of Crystal Growth 3, Thin Films and Epitaxy, Part B. Growth Mechanics and Dynamics, Atomic Layer Epitaxy*; Elsevier: Amsterdam, 1994.
(12) Devine, R. A. B.; Chaneliere, C.; Autran, J. L.; Balland, B.; Paillet, P.; Leray, J. L. *Microelectron. Eng.* **1997**, *36*, 61.
(13) Koyama, H.; Tanimoto, S.; Kuroiwa, K.; Tarui, Y. *Jpn. J. Appl. Phys.* **1994**, *33*, 6291.
(14) (a) Aarik, J.; Aidla, A.; Kukli, K.; Uustare, T. *J. Cryst. Growth* **1994**, *75*, 180. (b) Kukli, K.; Aarik, J.; Aidla, A.; Kohan, O.; Uustare, T.; Sammelselg, V. *Thin Solid Films* **1995**, *260*, 135. (c) Simon, H.; Aarik, J. *J. Phys. IV* **1995**, *5*, C5−277. (d) Aarik, J.; Kukli, K.; Aidla, A.; Pung, L. *Appl. Surf. Sci.* **1996**, *103*, 331.
(15) (a) Doren, D. J. In *Advances in Chemical Physics, Vol. XCV*; Progogine, I., Rice, S. A., Eds.; Wiley: New York, 1996; p 1. (b) Simka, H.; Hierlemann, M.; Ulz, M.; Jensen, K. F. *J. Electrochem. Soc.* **1996**, *143*, 2646. (c) Hierlemann, M.; Werner, C.; Spitzer, A. *J. Vac. Sci. Technol. B.* **1997**, *15*, 935. (d) Ho, P.; Colvin, M. E.; Melius, C. E. *J. Phys. Chem.* **1997**, *101*, 9470. (e) Harris, S. J.; Kiefer, J.; Zhang Q.; Schoene, A.; Lee, K.-W. *J. Electrochem. Soc.* **1998**, *145*, 3203. (f) Allendirf, M. D.; Teyssandlier, F. *J. Electrochem. Soc.* **1998**, *145*, 2167. (g) Korkin, A. A.; Cole, J. V.; Sengupta, D.; Adams, J. B. *J. Electrochem. Soc.* **1999**, *146*, 4203.
(16) The preliminary results were presented at E-MRS 1999 Spring Meeting in Strasbourg, 1−4 June 1999.
(17) Frenking, G.; Antes, I.; Böhme, M.; Dapprich, S.; Ehlers, A. W.; Jonas, V.; Neuhaus A.; Otto, M.; Stegmann, R.; Veldkamp, A.; Vyboishchikov, S. F. *Rev. Computat. Chem.* **1996**, *8*, 63 and references cited there.
(18) Ischenko, A. A.; Strand, T. G.; Demidov, A. V.; Spiridonov, V. P. *J. Mol. Struct.* **1978**, *43*, 227.
(19) Kang, S. K.; Tang, H.; Albright, T. A. *J. Am. Chem. Soc.* **1993**, *115*, 1971.
(20) Benson, M. T.; Cundari, T. R.; Li, Yu; Strohecker, L. A. *Int. J. Quantum Chem.: Quantum Chem. Symp.* **1994**, *28*, 181.
(21) Deng, L.; Ziegler, T. *Organometallics* **1996**, *15*, 3011.
(22) (a) Møller, C.; Plesset, M. S. *Phys. Rev.* **1934**, *46*, 618. (b) Binkley, J. S.; Pople, J. A. *Int. J. Quantum Chem.* **1975**, *9S*, 229.
(23) Becke, A. D. *J. Chem. Phys.* **1993**, *98*, 5648.
(24) Frisch, M. J.; Trucks, G. W.; Schlegel, H. B.; Secures, G. E.; Robb, M. A.; Cheeseman, J. R.; Zakrzewski, V. G.; Montgomery, J. A. Jr.; Stratmann, R. E.; Burant, J. C.; Dapprich, S.; Millam, J. M.; Daniels, A. D.; Kudin, K. N.; Strain, M. C.; Farkas, O.; Tomasi, J.; Barone, V.; Cossi, M.; Cammi, R.; Mennucci, B.; Pomelli, C.; Adamo, C.; Clifford, S.; Ochterski, J.; Petersson, G. A.; Ayala, P. Y.; Cui, Q.; Morokuma, K.; Malick, D. K.; Rabuck, A. D.; Raghavachari, K.; Foresman, J. B.; Cioslowski, J.; Ortiz, J. V.; Stefanov, B. B.; Liu, G.; Liashenko, A.; Piskorz, P.; Komaromi, I.; Gomperts, R.; Martin, R. L.; Fox, D. J.; Keith, T.; Al-Laham, M. A.; Peng, C. Y.; Nanayakkara, A.; Gonzalez, C.; Challacombe, M.; Gill, P. M. W.; Johnson, B.; Chen, W.; Wong, M. W.; Andres, J. L.; Gonzalez, C.; Head-Gordon, M.; Replogle, E. S.; Pople, J. A. *Gaussian 98*, Revision A.3; Gaussian, Inc.: Pittsburgh, PA, 1998.
(25) Hehre, W. J.; Radom, L.; Pople, J. A.; Schleyer, P. v. R. *Ab Initio Molecular Orbital Theory*; Wiley: New York, 1986.
(26) (a) Cizek, J.; *J. Chem. Phys.* **1966**, *45*, 4256. (b) Pople, J. A.; Krishnan, R.; Schlegel, H. B.; Binkley, J. S. *Int. J. Quantum Chem.* **1978**, *14*, 545. (c) Bartlett, R. J.; Purvis, G. D. *Int. J. Quantum Chem.* **1978**, *14*, 561. (d) Purvis, G. D.; Bartlett, R. J. *J. Chem. Phys.* **1982**, *76*, 1910. (e) Raghavachari, K.; Trucks, G. W.; Pople, J. A.; Head-Gordon, M. *Chem. Phys. Lett.* **1989**, *157*, 479. (f) Bartlett, R. J.; Watts, J. D.; Kucharski, S. A.; Noga, J. *Chem. Phys. Lett.* **1990**, *165*, 513.
(27) Hay, P. J.; Wadt, W. R. *J. Chem. Phys.* **1985**, *82*, 299.
(28) Bergner, A.; Dolg, M.; Kuechle; W., Stoll, H.; Preuss, H. *Mol. Phys.* **1993**, *80*, 1413.
(29) Huzinaga, S. *Gaussian basis sets for molecular calculations*; Elsevier: Amsterdam, Oxford, New York, Tokyo, 1984.
(30) (a) Ditchfield, R.; Hehre, W. J.; Pople, J. A. *J. Chem. Phys.* **1971**, *54*, 724. (b) Hariharan, P. C.; Pople, J. A. *Theor. Chim. Acta* **1973**, *28*, 213. (c) Francl, M. M.; Pietro, W. J.; Hehre, W. J.; Binkley, J. S.; Gordon, M. S.; DeFrees, D. J.; Pople, J. A. *J. Chem. Phys.* **1982**, *77*, 3654.
(31) Russo, T. V.; Martin, R. L.; Hay, P. J. *J. Phys. Chem.* **1995**, *99*, 17085.
(32) (a) *Spectroscopic Properties of Inorganic and Organometallic Compounds*; The Royal Society of Chemistry, Garden City Press Limited: London, 1984; Vol. 16, p 762. (b) Dobs, K. D.; Hehre, W. J. *J. Comput. Chem.* **1987**, *8*, 861. (c) Benson, M. T.; Cundari, T. R.; Lim, S. J.; Nguyen, H. D.; Pierce-Beaver, K. *J. Am. Chem. Soc.* **1994**, *116*, 3966. (d) Sosa, C.; Andzelm, J.; Elkins, B. C.; Wimmer, E.; Dobbs, K. D.; Dixon, D. A. *J. Phys. Chem.* **1992**, *96*, 6630. (e) Russo, T. V.; Martin, R. L.; Hay, P. J. *J. Chem. Phys.* **1995**, *102*, 9315.
(33) Rosenkilde, C.; Voyiatzis, G.; Jensen, V. R.; Ystens, M.; Østvold, T. *Inorg. Chem.* **1995**, *34*, 4360.
(34) (a) *Structure Data of Free Polyatomic Molecules*; Springer: Berlin, 1987. (b) *Modern Organic Chemistry*; Marcel Dekker: New York, 1973; p 421.
(35) Figueira, R. R.; Fournier, L. L.; Varetti, E. L. *Spectrochim. Acta Part A* **1982**, *38*, 965.
(36) Beattie, I. R.; Livingstone, K. M. S.; Reynolds, D. J.; Ozin, G. A. *J. Chem. Soc. A.* **1970**, 1210.
(37) Landis, C. R.; Cleveland, T.; Firman, T. K *J. Am. Chem. Soc.* **1995**, *117*, 1859.
(38) Del Bene, J. E.; Person, W. B.; Szczepaniak, K. *J. Phys. Chem.* **1995**, *99*, 9, 10705.
(39) Chase, M. W. *NIST-JANAF Thermochemical Tables, Fourth Edition, J. Phys. Chem. Ref. Data, Monograph 9*, 1998.
(40) Lubin, L.; Liting, Li, Tobin, J. M. *J. Am. Chem. Soc.* **1997**, *119*, 8574.
(41) Acho, J. A.; Doerrer, L. H.; Lipppard, S. J. *Inorg. Chem.* **1995**, *34*, 2542.
(42) (a) Zielinski, J. J.; Poirier, R. A.; Peterson, M. R.; Csizmadia, I. G. *J. Comput. Chem.* **1983**, *4*, 419. (b) Nguyen, M. T.; Ha, T.-K. *J. Am. Chem. Soc.* **1984**, *106*, 599. (c) Nguyen, M. T.; Hegarty, A. F.; *J. Am. Chem. Soc.* **1984**, *106*, 1552. (d) McKee, M. L. *J. Phys. Chem.* **1993**, *97*, 13608.